

Multi-scale dynamics simulations of molecular polaritons: The effect of multiple cavity modes on polariton relaxation

Cite as: J. Chem. Phys. 154, 104112 (2021); doi: 10.1063/5.0037868

Submitted: 16 November 2020 • Accepted: 10 February 2021 •

Published Online: 9 March 2021



Ruth H. Tichauer,¹  Johannes Feist,²  and Gerrit Groenhof^{1,a)} 

AFFILIATIONS

¹Nanoscience Center and Department of Chemistry, University of Jyväskylä, P.O. Box 35, 40014 Jyväskylä, Finland

²Departamento de Física Teórica de la Materia Condensada and Condensed Matter Physics Center (IFIMAC), Universidad Autónoma de Madrid, Madrid, Spain

Note: This paper is part of the JCP Special Topic on Polariton Chemistry: Molecules in Cavities and Plasmonic Media.

a) Author to whom correspondence should be addressed: gerrit.x.groenhof@jyu.fi

ABSTRACT

Coupling molecules to the confined light modes of an optical cavity is showing great promise for manipulating chemical reactions. However, to fully exploit this principle and use cavities as a new tool for controlling chemistry, a complete understanding of the effects of strong light–matter coupling on molecular dynamics and reactivity is required. While quantum chemistry can provide atomistic insight into the reactivity of uncoupled molecules, the possibilities to also explore strongly coupled systems are still rather limited due to the challenges associated with an accurate description of the cavity in such calculations. Despite recent progress in introducing strong coupling effects into quantum chemistry calculations, applications are mostly restricted to single or simplified molecules in ideal lossless cavities that support a single light mode only. However, even if commonly used planar mirror micro-cavities are characterized by a fundamental mode with a frequency determined by the distance between the mirrors, the cavity energy also depends on the wave vector of the incident light rays. To account for this dependency, called cavity dispersion, in atomistic simulations of molecules in optical cavities, we have extended our multi-scale molecular dynamics model for strongly coupled molecular ensembles to include multiple confined light modes. To validate the new model, we have performed simulations of up to 512 Rhodamine molecules in red-detuned Fabry–Pérot cavities. The results of our simulations suggest that after resonant excitation into the upper polariton at a fixed wave vector, or incidence angle, the coupled cavity–molecule system rapidly decays into dark states that lack dispersion. Slower relaxation from the dark state manifold into both the upper and lower bright polaritons causes observable photo-luminescence from the molecule–cavity system along the two polariton dispersion branches that ultimately evolves toward the bottom of the lower polariton branch, in line with experimental observations. We anticipate that the more realistic cavity description in our approach will help to better understand and predict how cavities can modify molecular properties.

Published under license by AIP Publishing. <https://doi.org/10.1063/5.0037868>

I. INTRODUCTION

Recent experiments that demonstrate tuning of chemical reactivity through strong light–matter interactions within optical micro-cavities have greatly revived the interest in cavity polaritons.^{1–7} Polaritons are hybrid light–matter states that emerge as the normal modes of a system consisting of a cavity photon and a material excitation that interact in the strong coupling regime. This regime

is reached when the interaction strength between the cavity photon and material excitation exceeds the rates of both photon and excitation damping processes and is manifested by a Rabi splitting of the absorption spectrum.^{8–11}

Cavity polaritons have been thoroughly investigated for decades, in particular, within inorganic semiconductor micro-cavities.¹² Although the inherent disorder and large exciton linewidths of organic media have for long restricted the study of

such materials to the weak coupling regime,^{13,14} the identification of suitable organic molecules, with narrow and intense optical transitions, made it possible to reach the strong coupling regime in such media as well and observe the characteristic anti-crossing between the upper and lower polaritons.^{15–22} Moreover, because Frenkel excitons in organic molecules have much larger oscillator strengths than Wannier–Mott excitons in inorganic semiconductors, the Rabi splitting of organic micro-cavities easily exceeds that of inorganic micro-cavities and can even be observed at room temperature.^{15–19,21,22}

Although the fundamental signatures of the strong coupling regime are evident, the inherent disorder of organic planar mirror (Fabry–Pérot) micro-cavities gives rise to features that are absent in their inorganic counterparts.^{23,24} Indeed, because of dissipation processes taking place within organic molecules, both the energy and wave vector, \mathbf{k} , of the polaritonic states emerging under strong coupling are broadened. This broadening is such that at the end-points, i.e., $|\mathbf{k}| \rightarrow 0$ and $|\mathbf{k}| \rightarrow \infty$, a wide range of wave-vector values $|\mathbf{k}|$ can be attributed to the same polaritonic energy level, causing a large uncertainty in the wave vector associated with states in these regions of the cavity spectrum. Consequently, these states can no longer be described by the wave vector, and therefore, the range of \mathbf{k} associated with the upper polariton (UP) or lower polariton (LP) is reduced compared to polariton branches emerging within inorganic systems.

Furthermore, according to the uncertainty principle, the large uncertainty in momentum allows for spatial localization.^{25,26} Therefore, in a strongly coupled organic micro-cavity, both coherent (delocalized) and incoherent (localized) excited states coexist. Whereas the coherent states have a well-defined wave vector, \mathbf{k} , and belong to the usual polariton branches provided that $|\mathbf{k}_{\min}^{\text{LP}}| < |\mathbf{k}| < |\mathbf{k}_{\max}^{\text{LP}}|$ for the LP and $|\mathbf{k}| > |\mathbf{k}_{\min}^{\text{UP}}|$ for the UP, the incoherent states are either (i) similar add-mixtures of photonic and molecular excitations such that when their photonic component is small, they are referred to as *dark states* or (ii) purely molecular excitations that are not coupled (or weakly coupled) to the cavity photon, yet visible in the photo-luminescence spectra as they decay through (enhanced) spontaneous emission.¹⁹

Despite experimental^{15–19,21,22,27} and theoretical work^{23,25,26,28–35} on organic micro-cavities, the microscopic understanding of polariton dynamics within such media remains incomplete. In previous analytical^{23,28,29,34} and numerical approaches,^{36–38} polariton relaxation was studied using either a simplified description of the molecules as two-level systems^{23,28,29} or as harmonic oscillators,^{34,35} a single confined light mode rather than the full cavity dispersion,^{36,38,39} or a combination of both.^{30–32,37,40,41} While the simplified description of the molecules precludes modeling chemical reactivity, neglecting the cavity dispersion prevents a realistic description of polariton relaxation in simulations.

To model the effect of strong coupling between molecules and a *single* cavity mode on chemical reactivity, we had previously developed a multi-scale molecular dynamics approach based on a hybrid Quantum Mechanics/Molecular Mechanics (QM/MM) description⁴² of the molecules and their chemical environment.^{36,38} To go beyond the single mode approximation, which is necessary for a realistic description of cavity-modified chemistry, we have extended our approach to include the multiple radiation modes that span the cavity dispersion. With the extended model, we have

simulated the relaxation dynamics of an organic micro-cavity system with 16 modes and containing up to 512 Rhodamine chromophores, after resonant photo-excitation into the UP at a fixed angle between the cavity and the laser beam.

This paper is organized as follows: First, in Sec. II, we explain how we include multiple cavity modes into our Tavis–Cummings based multi-scale molecular dynamics model.³⁶ Then, in Sec. III, we provide details and the parameters of the atomistic Rhodamine micro-cavity simulations, followed by a presentation and discussion of the results of these simulations in Sec. IV. We conclude our paper in Sec. V with an outlook.

II. THEORY

Following Michetti and La Rocca,²⁹ we assume that our cavity is two dimensional (2D), as illustrated in Fig. 1. When probed with a ray of light, photons entering the cavity have an energy,

$$\hbar\omega_{\text{cav}}(\mathbf{k}) = \frac{\hbar c|\mathbf{k}|}{n_r} = \frac{\hbar c}{n_r} \sqrt{k_x^2 + k_z^2}, \quad (1)$$

where \hbar is the reduced Planck constant, c is the speed of light, and n_r is the refractive index of the propagation media. The mirrors at $-\frac{1}{2}x$ and $\frac{1}{2}x$ confine light along the x axis to discrete wave vectors ($k_x = m\pi/L_x$ with $m \in \mathbb{N}$ and $L_x = x$ is the cavity width) and thus set the cavity resonance at zero incidence ($k_z = 0$) to $\omega_0 = m\pi c/(n_r L_x)$. Because we restrict m to 1, the first cavity mode, the energy of the cavity photon depends solely on the z -component of the incident wave vector: $\hbar\omega_{\text{cav}}(k_z)$. Therefore, the multiple modes that arise from

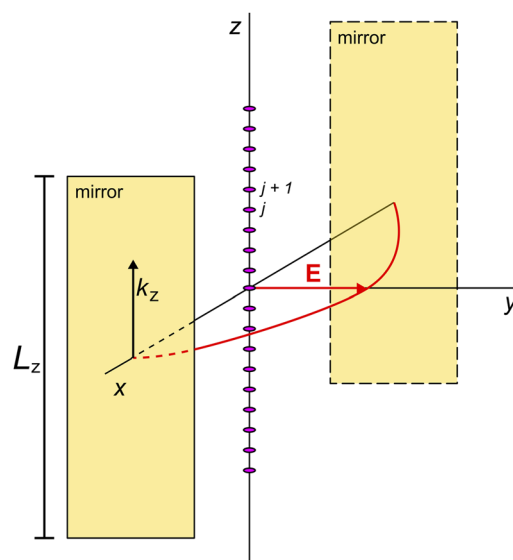


FIG. 1. Two dimensional (2D) Fabry–Pérot cavity model. Two reflecting mirrors are located at $-\frac{1}{2}x$ and $\frac{1}{2}x$, confining light modes along this direction, while free propagation along the z -direction is possible for plane waves with in-plane momentum k_z and energy $\hbar\omega(k_z)$. The vacuum field vector (red) points along the y axis, reaching a maximum amplitude at $x = 0$ where the N molecules (magenta ellipses) are placed, distributed along the z axis at positions z_j with $1 \leq j \leq N$.

the dependence of the cavity energy on the wave vector are fully characterized by k_z .

Inside the cavity, N molecules are located on the z axis with their geometrical centers at positions z_j (Fig. 1). To model the interactions between these molecules and the micro-cavity modes, we make the rotating wave approximation (RWA) and include these modes into the Tavis–Cummings Hamiltonian,^{29,43,44}

$$\begin{aligned} \hat{H}^{\text{TC}} = & \sum_j \hbar \nu_j(\mathbf{R}_j) \hat{\sigma}_j^+ \hat{\sigma}_j^- + \sum_{k_z} \hbar \omega_{\text{cav}}(k_z) \hat{a}_{k_z}^\dagger \hat{a}_{k_z} \\ & + \sum_j \sum_{k_z} \hbar g_j(k_z) \left(\hat{\sigma}_j^+ \hat{a}_{k_z} \mathbf{f}_z(z_j) + \hat{\sigma}_j^- \hat{a}_{k_z}^\dagger \mathbf{f}_z^*(z_j) \right) \\ & + \sum_i V_{S_0}(\mathbf{R}_i). \end{aligned} \quad (2)$$

Here, $\hat{\sigma}_j^+$ ($\hat{\sigma}_j^-$) is the operator that excites (de-excites) molecule j from the electronic ground (excited) state $|S_0^j(\mathbf{R}_j)\rangle$ ($|S_1^j(\mathbf{R}_j)\rangle$) to the electronic excited (ground) state $|S_1^j(\mathbf{R}_j)\rangle$ ($|S_0^j(\mathbf{R}_j)\rangle$); \mathbf{R}_j is the vector of the Cartesian coordinates of all atoms in molecule j ; \hat{a}_{k_z} ($\hat{a}_{k_z}^\dagger$) is the annihilation (creation) operator of a cavity photon with wave vector k_z ; $\mathbf{f}_z(z_j) = e^{ik_z z_j}$ is the function describing the form of the quantized electromagnetic (EM) field modes, here taken to be that of plane waves with in-plane momentum k_z ; and $\hbar \nu_j(\mathbf{R}_j)$ is the excitation energy of molecule j , defined as

$$\hbar \nu_j(\mathbf{R}_j) = V_{S_1}^{\text{mol}}(\mathbf{R}_j) - V_{S_0}^{\text{mol}}(\mathbf{R}_j), \quad (3)$$

with $V_{S_0}^{\text{mol}}(\mathbf{R}_j)$ and $V_{S_1}^{\text{mol}}(\mathbf{R}_j)$ the adiabatic potential energy surfaces of molecule j in the electronic ground (S_0) and excited (S_1) state, respectively. The last term in Eq. (2) is the total potential energy of the system in the absolute ground state (i.e., with no excitations in neither the molecules nor the cavity modes), defined as the sum of the ground-state potential energies of all molecules. As in previous work, we use a hybrid quantum mechanics/molecular mechanics (QM/MM) Hamiltonian⁴² to model these potentials.³⁶

The first sum in \hat{H}^{TC} runs over the N molecules, and the second sum runs over all cavity modes with photon energy $\hbar \omega_{\text{cav}}(k_z)$ [Eq. (1)]. The third term describes the light–matter interaction within the dipolar approximation through $g_j(k_z)$ that, differently from the case in which only the mode at normal incidence is taken into account (i.e., $k_z = 0$), not only depends on the transition dipole moment $\boldsymbol{\mu}_j$ of the molecules but also on the cavity mode wave vector k_z ,

$$g_j(k_z) = -\boldsymbol{\mu}_j(\mathbf{R}_j) \cdot \mathbf{u}_{\text{cav}} \sqrt{\frac{\hbar \omega_{\text{cav}}(k_z)}{2\epsilon_0 V_{\text{cav}}}}, \quad (4)$$

where \mathbf{u}_{cav} is the unit vector indicating the direction of the electric component of the confined mode, here along the y -direction (Fig. 1); ϵ_0 is the vacuum permittivity; and V_{cav} is the volume into which the mode with in-plane momentum k_z is confined. The transition dipole moments of the molecules, as well as their excitation energies, $\hbar \nu_j(\mathbf{R}_j)$, depend only on the molecular geometry, \mathbf{R}_j .

As in Michetti and La Rocca,²⁹ we impose periodic boundary conditions in the z -direction and thus restrict the plane-wave

solutions of Maxwell’s equation to

$$\begin{aligned} \mathbf{f}_z(z) &= \mathbf{f}_z(z + L_z), \\ e^{izk_z} &= e^{i(z+L_z)k_z}, \\ e^{iL_z k_z} &= 1. \end{aligned} \quad (5)$$

To satisfy these boundary conditions, the wave vectors, k_z , must have discrete values: $k_z = 2\pi n/L_z$ with $n \in \mathbb{Z}$ and L_z is the length of the cavity (Fig. 1).

Because modes that are much higher in energy than the molecular excitation energies ($\hbar \nu_j$), hardly couple with the molecules under the RWA, we furthermore neglect modes above an energy threshold, $\hbar \omega_{\text{cav}}(2\pi n_{\text{max}}/L_z)$, sufficiently above the molecular excitation. Thus, the number of modes included in our description is limited by n_{max} . As in Michetti and La Rocca,²⁹ we avoid degeneracies by excluding modes with negative wave vectors (i.e., $k_z < 0$ or $n < 0$). Therefore, the first mode included in our simulation model corresponds to the lowest energy mode ($\hbar \omega_0$), which is excited by light entering the cavity at normal incidence (i.e., $k_z = 0$ or $n_{\text{min}} = 0$).

With these approximations and under the additional assumption that the system is within the single-excitation subspace accessed under weak driving, the molecular Tavis–Cummings Hamiltonian in Eq. (2) can be represented as a $(N + n_{\text{max}} + 1)$ by $(N + n_{\text{max}} + 1)$ matrix with four blocks,

$$\mathbf{H}^{\text{TC}} = \begin{pmatrix} \mathbf{H}^{\text{mol}} & \mathbf{H}^{\text{int}} \\ \mathbf{H}^{\text{int}\dagger} & \mathbf{H}^{\text{cav}} \end{pmatrix}. \quad (6)$$

The upper left block, \mathbf{H}^{mol} , is a $N \times N$ matrix containing the single-photon excitations of the molecules. Because at the molecular concentrations considered here, direct interactions between photoactive molecules can be neglected, the molecular block is diagonal, with elements labeled by the molecule indices j ,

$$\begin{aligned} H_{jj}^{\text{mol}} &= \langle 0 | \langle S_0^1(\mathbf{R}_1) S_0^2(\mathbf{R}_2) \dots S_1^j(\mathbf{R}_j) \dots S_0^N(\mathbf{R}_N) | \hat{H}^{\text{TC}} | S_0^1(\mathbf{R}_1) \\ &\quad \times S_0^2(\mathbf{R}_2) \dots S_1^j(\mathbf{R}_j) \dots S_0^N(\mathbf{R}_N) \rangle | 0 \rangle, \end{aligned} \quad (7)$$

for $1 \leq j \leq N$. Each matrix element of \mathbf{H}^{mol} thus represents the potential energy of molecule j in the electronic excited state $|S_1^j(\mathbf{R}_j)\rangle$ and all other molecules $i \neq j$ in the electronic ground states $|S_0^i(\mathbf{R}_i)\rangle$,

$$H_{jj}^{\text{mol}} = V_{S_1}^{\text{mol}}(\mathbf{R}_j) + \sum_{i \neq j} V_{S_0}^{\text{mol}}(\mathbf{R}_i). \quad (8)$$

The $|0\rangle$ in Eq. (7) indicates that the single-photon Fock states of all cavity modes are empty.

The lower right block, \mathbf{H}^{cav} , is a $(n_{\text{max}} + 1) \times (n_{\text{max}} + 1)$ matrix containing the single-photon excitations of the cavity modes. Because the plane-wave basis set is orthogonal, there are no direct interactions between cavity modes and thus the cavity mode excitation block in the Tavis–Cummings Hamiltonian [Eq. (6)] is diagonal as well, with elements labeled by the mode indices b ,

$$\begin{aligned} H_{b,b}^{\text{cav}} &= \langle 1_b | \langle S_0^1(\mathbf{R}_1) S_0^2(\mathbf{R}_2) \dots S_0^N(\mathbf{R}_N) | \hat{H}^{\text{TC}} | S_0^1(\mathbf{R}_1) \\ &\quad \times S_0^2(\mathbf{R}_2) \dots S_0^N(\mathbf{R}_N) \rangle | 1_b \rangle, \end{aligned} \quad (9)$$

for $0 \leq b \leq n_{\max}$. Here, $|1_b\rangle$ indicates the single-photon Fock state of cavity mode b with wave vector $k_z = 2\pi b/L_z$. In these matrix elements, all molecules are in the electronic ground state (S_0), while mode b is excited. The energy is, therefore, the sum of the molecular ground state energies *plus* the cavity energy at k_z , which follows the dispersion relation [Eq. (1)],

$$H_{b,b}^{\text{cav}} = \hbar\omega_{\text{cav}}(2\pi b/L_z) + \sum_j^N V_{S_0}^{\text{mol}}(\mathbf{R}_j). \quad (10)$$

The two $N \times (n_{\max} + 1)$ off-diagonal blocks \mathbf{H}^{int} and $\mathbf{H}^{\text{int}\dagger}$ in the multi-mode Tavis–Cummings Hamiltonian [Eq. (6)] describe the interactions between the molecules and the cavity modes. These matrix elements are approximated as the overlap between the transition dipole moment of the electronically excited molecule j and the electric field of the cavity mode b [Eq. (4)],

$$H_{j,b}^{\text{int}} = -\boldsymbol{\mu}_j(\mathbf{R}_j) \cdot \mathbf{u}_{\text{cav}} \sqrt{\frac{\hbar\omega_{\text{cav}}(2\pi b/L_z)}{2\epsilon_0 V_{\text{cav}}}} \times \langle 0_b | \langle S_1 | \hat{\sigma}_j^+ \hat{a}_b e^{i2\pi b z_j/L_z} | S_0^j \rangle | 1_b \rangle, \quad (11)$$

for $1 \leq j \leq N$ and $0 \leq b \leq n_{\max}$. Because molecules are typically much smaller than the width (L_x) of a Fabry–Pérot micro-cavity, variations in the cavity field strength over the dimension of the molecules are neglected. Furthermore, excitonic interactions between molecules are also neglected, which is strictly valid for low molecular concentrations only. For simulations at higher chromophore concentrations, excitonic interactions between the molecules can be included via a multi-pole expansion of the molecular transition densities, as in excitonic models.⁴⁵

The multiple cavity-mode Tavis–Cummings Hamiltonian [Eq. (6)] is diagonalized at each time step of a Molecular Dynamics (MD) simulation to obtain the $N + n_{\max} + 1$ (*adiabatic*) polaritonic eigenstates and energies. These eigenstates are coherent superpositions of electronic excitations in the N molecules and of the $n_{\max} + 1$ cavity modes,

$$\psi^m = \sum_j^N \beta_j^m |S_0^1 S_0^2 \dots S_1^j \dots S_0^{N-1} S_0^N\rangle |0\rangle + \sum_{b=0}^{n_{\max}} \alpha_b^m |S_0^1 S_0^2 \dots S_0^j \dots S_0^{N-1} S_0^N\rangle |1_b\rangle, \quad (12)$$

where the index m labels the $N + n_{\max} + 1$ single-photon polaritonic eigenstates of the strongly coupled molecule–cavity system with eigenenergies E_m , while β_j^m and α_b^m are the expansion coefficients ($\sum_j |\beta_j^m|^2 + \sum_b |\alpha_b^m|^2 = 1$) that determine the contributions of each molecular excitation (S_1^j) and each cavity mode (b) to polariton ψ^m .

Trajectories of all atoms in each molecule are computed by numerically integrating Newton’s equations of motion. Because in systems with many molecules and modes, the eigenstates span an almost degenerate manifold,³⁹ non-adiabatic couplings \mathbf{d}_{ml} , which are inversely proportional to the energy gap between polaritonic states m and l ,

$$\mathbf{d}_{ml} = \langle \psi^m | \nabla_a \psi^l \rangle = \frac{\langle \psi^m | \nabla_a \hat{H}^{\text{TC}} | \psi^l \rangle}{E_l - E_m} \quad (13)$$

can induce population transfer between these states during the dynamics. Here, a indicates an atom in one of the N molecules. In our approach, such transfers can be modeled either by discrete surface hops between the polaritonic states^{46–48} or by classically evolving the trajectory on the mean-field potential energy surface.^{38,49} In both cases, the polaritonic wave function is coherently propagated along with the classical degrees of freedom as a time-dependent superposition of the $N + n_{\max} + 1$ time-independent *adiabatic* polaritonic states,

$$\Psi(t) = \sum_m^{N+n_{\max}+1} c_m(t) \psi^m, \quad (14)$$

where $c_m(t)$ are the time-dependent expansion coefficients of the time-independent polaritonic basis functions [Eq. (12)]. These coefficients are evolved along the trajectory of the N molecules, using the unitary propagator in the *local* diabatic basis.^{38,50}

The Hellman–Feynman gradients, $\langle \psi^m | \nabla_a \hat{H}^{\text{TC}} | \psi^l \rangle$, required for classically propagating the nuclear degrees of freedom in the Ehrenfest mean-field formalism, or for computing the non-adiabatic coupling vectors (\mathbf{d}_{ml}) in fewest switches surface hopping simulations,^{46,47} are obtained as before³⁸ but taking into account that the polaritonic expansion coefficients [i.e., β_j^m and α_b^m in Eq. (12)] are now complex,

$$\begin{aligned} \langle \psi^m | \nabla_a \hat{H}^{\text{TC}} | \psi^l \rangle &= \sum_k^N \sum_j^N (\beta_k^m)^* \beta_j^l \nabla_a H_{k,j}^{\text{mol}} \\ &+ \sum_b^{n_{\max}} \sum_d^{n_{\max}} (\alpha_b^m)^* \alpha_d^l \nabla_a H_{b,d}^{\text{cav}} \\ &+ \sum_k^N \sum_d^{n_{\max}} (\beta_k^m)^* \alpha_d^l \nabla_a H_{k,d}^{\text{int}} \\ &+ \sum_b^{n_{\max}} \sum_j^N (\alpha_b^m)^* \beta_j^l \nabla_a H_{b,j}^{\text{int}\dagger}. \end{aligned} \quad (15)$$

Because the molecular and cavity blocks of the Tavis–Cummings Hamiltonian are diagonal [Eq. (6)], the first two terms on the right-hand side of this equation are zero unless $k = j$ and $b = d$,

$$\begin{aligned} \langle \psi^m | \nabla_a \hat{H}^{\text{TC}} | \psi^l \rangle &= \sum_j^N (\beta_j^m)^* \beta_j^l \nabla_a H_{j,j}^{\text{mol}} + \sum_b^{n_{\max}} (\alpha_b^m)^* \alpha_b^l \nabla_a H_{b,b}^{\text{cav}} \\ &+ \sum_k^N \sum_d^{n_{\max}} (\beta_k^m)^* \alpha_d^l \nabla_a H_{k,d}^{\text{int}} \\ &+ \sum_b^{n_{\max}} \sum_j^N (\alpha_b^m)^* \beta_j^l \nabla_a H_{b,j}^{\text{int}\dagger}. \end{aligned} \quad (16)$$

For an atom a that is part of molecule j , this expression further simplifies to

$$\begin{aligned}
& \langle \psi^m | \nabla_{a \in j} \hat{H}^{\text{TC}} | \psi^l \rangle \\
&= (\beta_j^m)^* \beta_j^l \nabla_{a \in j} V_{S_1}^{\text{mol}}(\mathbf{R}_j) + \nabla_{a \in j} V_{S_0}^{\text{mol}}(\mathbf{R}_j) \\
&\quad \times \left[\sum_b^{n_{\text{max}}} (\alpha_b^m)^* \alpha_b^l + \sum_{k \neq j}^N (\beta_k^m)^* \beta_k^l \right] - (\beta_j^m)^* \nabla_{a \in j} \sum_b^{n_{\text{max}}} \\
&\quad \cdot \mathbf{u}_{\text{cav}} \sum_b^{n_{\text{max}}} (\alpha_b^l) \sqrt{\frac{\hbar \omega_{\text{cav}} (2\pi b / L_z)}{2\epsilon_0 V_{\text{cav}}}} e^{2\pi i b z_j / L_z} \\
&\quad - \beta_j^l \nabla_{a \in j} \boldsymbol{\mu}_j \cdot \mathbf{u}_{\text{cav}} \sum_b^{n_{\text{max}}} (\alpha_b^m)^* \sqrt{\frac{\hbar \omega_{\text{cav}} (2\pi b / L_z)}{2\epsilon_0 V_{\text{cav}}}} e^{-2\pi i b z_j / L_z}. \quad (17)
\end{aligned}$$

Finally, because the polaritonic eigenstates are orthonormal ($\sum_j^N (\beta_j^m)^* \beta_j^l + \sum_{b=0}^{n_{\text{max}}} (\alpha_b^m)^* \alpha_b^l = \delta_{ml}$), we can replace the sums between the square brackets in the second term on the right-hand side,

$$\begin{aligned}
& \langle \psi^m | \nabla_{a \in j} \hat{H}^{\text{TC}} | \psi^l \rangle \\
&= (\beta_j^m)^* \beta_j^l \nabla_{a \in j} V_{S_1}^{\text{mol}}(\mathbf{R}_j) + \nabla_{a \in j} V_{S_0}^{\text{mol}}(\mathbf{R}_j) \\
&\quad \times \left[\delta_{ml} - (\beta_j^m)^* \beta_j^l \right] - (\beta_j^m)^* \nabla_{a \in j} \boldsymbol{\mu}_j \cdot \mathbf{u}_{\text{cav}} \sum_b^{n_{\text{max}}} (\alpha_b^l) \\
&\quad \times \sqrt{\frac{\hbar \omega_{\text{cav}} (2\pi b / L_z)}{2\epsilon_0 V_{\text{cav}}}} e^{2\pi i b z_j / L_z} - \beta_j^l \nabla_{a \in j} \boldsymbol{\mu}_j \cdot \sum_b^{n_{\text{max}}} \\
&\quad \cdot \mathbf{u}_{\text{cav}} \sum_b^{n_{\text{max}}} (\alpha_b^m)^* \sqrt{\frac{\hbar \omega_{\text{cav}} (2\pi b / L_z)}{2\epsilon_0 V_{\text{cav}}}} e^{-2\pi i b z_j / L_z}. \quad (18)
\end{aligned}$$

Because the multi-mode Tavis–Cummings Hamiltonian \mathbf{H}^{TC} [Eq. (6)] contains only the single-excitation subspace, it assumes an ideal lossless cavity in which the zero-photon subspace [i.e., all molecules in the electronic ground state (S_0) and no photon in the cavity], accessed through photon emission (or non-radiative decay of a molecule to S_0), is not available. Thus, the cavity modes are assumed to have infinite lifetimes.

In reality, however, these lifetimes are limited by the quality factor of the cavity, Q , defined as

$$Q = \frac{\omega_{\text{cav}}}{\gamma_{\text{cav}}}, \quad (19)$$

where γ_{cav} is the dissipation rate of the confined light mode, which is the inverse of the cavity photon lifetime, $\tau_{\text{cav}} = 1/\gamma_{\text{cav}}$. In experiment, the Q factor depends on the accuracy of the nano-fabrication process, the thickness of the mirrors and the cavity material.⁵¹

In our simulations, spontaneous photon loss into the zero-photon subspace (i.e., the ground state of the system) is modeled as a first-order decay process of polaritonic states ψ^m with a non-zero photonic contribution [$\sum_{n=0}^{n_{\text{max}}} |\alpha_n^m|^2 > 0$ in Eq. (12)].³⁶ Under the assumption that the intrinsic decay rate γ_{cav} is the same for all modes, the polaritonic decay rate is calculated as the product of that intrinsic cavity decay rate γ_{cav} and the weight of the total photonic

contribution, $\sum_{n=0}^{n_{\text{max}}} |\alpha_n^m|^2$.³³ Thus, after an MD step Δt , we multiply the population ($\rho_m = c_m^* c_m$) of state ψ^m by

$$\rho_m(t + \Delta t) = \rho_m(t) \exp \left[-\gamma_{\text{cav}} \sum_n^{n_{\text{max}}} |\alpha_n^m(t)|^2 \Delta t \right]. \quad (20)$$

Because $\rho_m = (\Re[c_m])^2 + (\Im[c_m])^2$, the change in the real and imaginary parts of the (complex) expansion coefficients $c_m(t)$ due to spontaneous photonic loss in a low-finesse cavity are

$$\begin{aligned}
\Re[c_m(t + \Delta t)] &= \Re[c_m(t)] \exp \left[-\frac{1}{2} \gamma_{\text{cav}} \sum_n^{n_{\text{max}}} |\alpha_n^m(t)|^2 \Delta t \right], \\
\Im[c_m(t + \Delta t)] &= \Im[c_m(t)] \exp \left[-\frac{1}{2} \gamma_{\text{cav}} \sum_n^{n_{\text{max}}} |\alpha_n^m(t)|^2 \Delta t \right]. \quad (21)
\end{aligned}$$

Simultaneously, the population of the zero-excitation subspace, $\rho_0(t + \Delta t)$, increases

$$\rho_0(t + \Delta t) = \rho_0(t) + \sum_m \rho_m(t) \left(1 - \exp \left[-\gamma_{\text{cav}} \sum_n^{n_{\text{max}}} |\alpha_n^m(t)|^2 \Delta t \right] \right). \quad (22)$$

The multi-mode Tavis–Cummings model for atomistic molecular dynamics simulations of molecules in optical cavities was implemented in Gromacs 4.5.3 and is available for download from GitHub (https://github.com/rhti/gromacs_qed). Because the excited-state and ground-state energies as well as transition dipole moments can be computed for each molecule (plus environment) on a separate node of a computer cluster, and communication is limited to $3N$ double precision numbers per MD step, the approach is trivially parallel. Therefore, simulations of very large ensembles are feasible when sufficient computational resources are available.³⁶

III. SIMULATION DETAILS

We simulated ensembles of up to 512 Rhodamine molecules inside both lossless ($\gamma_{\text{cav}} = 0$ eV or 0 ps⁻¹) and lossy ($\gamma_{\text{cav}} = 0.04$ eV or 66.67 ps⁻¹) optical micro-cavities supporting 16 modes following the simulation workflow described below and depicted in Fig. S1 of the [supplementary material](#). The lifetimes of the lossy cavity systems were chosen to be comparable to the metallic Fabry–Pérot cavities that have been used in recent experiments on strong coupling with organic molecules.^{52,53}

A. Rhodamine model

The Rhodamine model, shown in Fig. 2, was modeled with the Amber03 force field,⁵⁴ using the parameters described by Luk *et al.*³⁶ This model was prepared for our simulations as follows (step 1 in the simulation workflow of the [supplementary material](#)): After a geometry optimization at the force field level, the molecule was placed at the center of a rectangular box filled with 3684 TIP3P water molecules.⁵⁵ The simulation box thus contained 11 089 atoms and was equilibrated for 2 ns with harmonic restraints on the heavy atoms of the Rhodamine molecule (force constant 1000 kJ mol⁻¹ nm⁻¹). Subsequently, a 200 ns classical molecular dynamics (MD) trajectory was computed at constant temperature (300 K) using a stochastic dynamics integrator with a friction coefficient of 0.1 ps⁻¹. The pressure was kept constant at 1 bar using the Berendsen isotropic pressure coupling algorithm⁵⁶ with a time constant of 1 ps. The LINCS algorithm was used to constrain

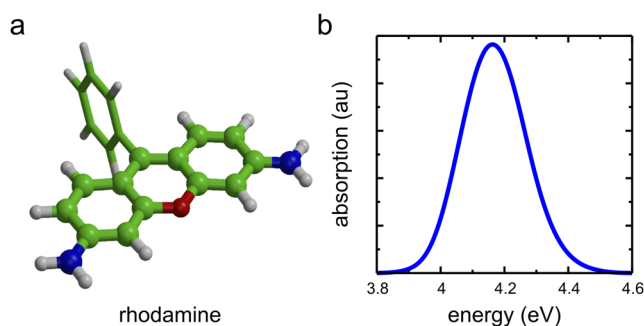


FIG. 2. (a) Rhodamine QM/MM model system. The QM atoms, treated at the RHF/3-21G and CIS/3-21G levels of theory for the ground (S_0) and excited states (S_1), respectively, are shown in ball-and-stick representation, while the MM atoms, modeled with the Amber03 force field,⁵⁴ are shown as sticks. The hydrogen link atom introduced along the bond on the QM/MM interface is not shown and neither are the 3684 TIP3P water molecules.⁵⁵ (b) QM/MM absorption spectrum of a Rhodamine ensemble. The absorption maximum at the CIS/3-21G//Amber03 level of theory is at 4.18 eV.

bond lengths,⁵⁷ while SETTLE was applied to constrain the internal degrees of freedom of the water molecules,⁵⁸ enabling a time step of 2 fs in the classical MD simulations. A 1.0 nm cutoff was used for van der Waals' interactions, which were modeled with Lennard-Jones potentials. Coulomb interactions were computed with the smooth particle mesh Ewald (PME) method,⁵⁹ using a 1.0 nm real space cutoff and a grid spacing of 0.12 nm. The relative PME tolerance at the real space cutoff was set to 10^{-5} .

The final configuration of the MM equilibration was subjected to a further 10 ps equilibration at the QM/MM level (step 2 in the simulation workflow of the [supplementary material](#)). The time step was reduced to 1 fs. As in previous work,³⁶ the fused ring system was included in the QM region and described at the RHF/3-21G level, while the rest of the molecule as well as the water solvent were modeled with the Amber03 force field⁵⁴ and the TIP3P water model,⁵⁵ respectively [Fig. 2(a)]. The bond connecting the QM and MM subsystems was replaced by a constraint, and the QM part was capped with a hydrogen atom. The force on the cap atom was distributed over the two atoms of the bond. The QM system experienced the Coulomb field of all MM atoms within a 1.6 nm cut-off sphere, and Lennard-Jones interactions between MM and QM atoms were added. The singlet electronic excited state (S_1) of the QM region was modeled with the configuration interaction method, truncated at single electron excitations (i.e., CIS/3-21G//Amber03). A comparison to more advanced (and costly) levels of theory in previous work³⁸ suggests that despite a significant overestimation of the excitation energy, CIS/3-21G yields potential energy surfaces that are in qualitative agreement with the more advanced approaches, including time-dependent density functional theory (TDDFT),⁶⁰ complete active space self-consistent field (CASSCF),⁶¹ and extended multi-configurational quasi-degenerate perturbation theory (xMC-QDPT2).⁶² Both MM and QM/MM simulations of Rhodamine outside of the cavity were performed with Gromacs 4.5.3⁶³ using the QM/MM interface to the TeraChem program^{64,65} (first and second steps in the simulation workflow of the [supplementary material](#)).

B. Molecular dynamics of cavity-molecule systems

The micro-cavity systems in this work were red-detuned, meaning that at zero incidence angle (i.e., $k_z = b = 0$), the energy of the cavity photon is below the absorption maximum of Rhodamine, which is 4.18 eV at the CIS/3-21G//Amber03 level of theory [Fig. 2(b)]. For the ideal lossless cavities, the cavity energy at zero incidence ($\hbar\omega_0$) was set to 3.81 eV, corresponding to a cavity width of $L_x = 0.163 \mu\text{m}$, while for the lossy cavities, it was set to 3.94 eV, corresponding to a cavity width of $0.157 \mu\text{m}$. For both micro-cavities, the cavity length was $L_z = 5 \mu\text{m}$, and the dispersion was modeled with 16 modes ($n_{\text{max}} = 15$), corresponding to an energy cutoff at 5.32 eV and 5.42 eV for the ideal and lossy cavities, respectively.

Both the cavity mode volume and the number of Rhodamine molecules were varied to yield Rabi splittings between 0.1 eV and 1 eV, in line with recent experiments.^{52,53,66–68} The molecules started from the same initial atomic coordinates but with different initial atomic velocities that were selected randomly from a Maxwell–Boltzmann distribution at a temperature of 300 K. With such initial conditions, the bright and dark polaritonic states can be unambiguously identified, while a rapid divergence due to the different starting velocities ensures sufficient energetic disorder among the molecules during the rest of the simulation. The molecules were oriented to maximize the coupling strength by aligning their transition dipole moments to the polarization of the vacuum field inside the cavity at the start of the simulations (i.e., \mathbf{E} in Fig. 1). Thus, in our simulations, the cavity contains no *uncoupled* molecules, which are assumed to be part of the so-called excitonic reservoir.²³

In one series of simulations, the geometric centers of the molecules were distributed evenly along the z axis of the cavity. To investigate also the effects of positional disorder,²⁹ we performed a second series of simulations in which the positions of the molecules were distributed randomly along the z axis. Because the number of eigenstates increases with the number of molecules and span a dense manifold, we use Ehrenfest dynamics, rather than the more popular fewest switches surface hopping algorithm,⁴⁶ to compute semi-classical MD trajectories, as in previous work.³⁸ The cavities were resonantly excited with a hypothetical $\delta(t, E)$ pulse into the UP branch near the k_z -vector where the cavity dispersion and molecular absorption maximum intersect. The integration time step for the classical molecular dynamics was further reduced to 0.1 fs. All cavity simulations were performed with Gromacs 4.5.3⁶³ in which the multi-mode Tavis–Cummings QM/MM model presented in Sec. II was implemented, using the QM/MM interface to TeraChem^{64,65} for ensembles with up until 128 molecules and to Gaussian16⁶⁹ for ensembles with over 128 molecules (third step in the simulation workflow of the [supplementary material](#)).

C. Photo-excitation and luminescence spectra

Following Lidzey and co-workers,¹⁸ we define the “visibility,” I^m , of polaritonic state ψ^m as the total photonic contribution to that state (i.e., $I^m \propto \sum_b^{n_{\text{max}}} |\alpha_b^m|^2$). Thus, the angle-resolved, or wave vector-dependent, one-photon absorption spectra of the Rhodamine–cavity systems were computed from the QM/MM trajectory of the uncoupled Rhodamine as follows: For each frame of this trajectory, the polaritonic states were computed and the energy

gaps of these states with respect to the overall ground state (i.e., E^0 , with all molecules in S_0 , no photon in the cavity: $|S_0^1 S_0^2 \dots S_0^N\rangle|0\rangle$) were extracted for all wave vectors, b , multiplied by $|\alpha_b^m|^2$ and summed up into a superposition of Gaussian functions,

$$I^{\text{abs}}(E, b) \propto \sum_i^S \left[\sum_m^{N+n_{\text{max}}+1} |\alpha_{b,i}^m|^2 \exp\left[-\frac{(E - \Delta E_i^m)^2}{2\sigma^2}\right] \right]. \quad (23)$$

Here, $I^{\text{abs}}(E, b)$ is the absorption intensity as a function of excitation energy E and in-plane momentum b ($k_z = 2\pi b/L_z$), S is the number of trajectory frames included in the analysis, ΔE_i^m is the excitation energy of polaritonic state m in frame i ($\Delta E_i^m = E_i^m - E_i^0$), and $\alpha_{b,i}^m$ is the expansion coefficient of cavity mode b in polaritonic state m in that frame [Eq. (12)]. A width of $\sigma = 0.05$ eV was chosen for all convolutions in this work.

Likewise, we also equate photo-luminescence intensity to the visibility for both the lossless and lossy cavities. Thus, the energy- and angle-resolved photo-luminescence spectra of the strongly coupled systems were computed as

$$I^{\text{pl}}(E, b) \propto \sum_i^S \left[\sum_m^{N+n_{\text{max}}+1} |c_m(t_i)|^2 |\alpha_{b,i}^m|^2 \exp\left[-\frac{(E - \Delta E_i^m)^2}{2\sigma^2}\right] \right], \quad (24)$$

where t_i is the time delay of MD step i with respect to the instantaneous photo-excitation at $t = 0$ and $|c_m(t_i)|^2$ is the population of polaritonic state ψ^m at t_i . As before, a width of $\sigma = 0.05$ eV was used to convolute the spectra.

We used Mathematica, version 11.3,⁷⁰ to create 2D plots of the convoluted angle-resolved absorption and photo-luminescence spectra. Because we sum over all states, the total intensity depends on the number of molecules in the cavity. To qualitatively compare photo-luminescence between cavities, the intensities were normalized for each system separately.

IV. RESULTS AND DISCUSSION

A. Molecules in ideal lossless cavities

To assess the effect of sample concentration on the molecular dynamics in the strong coupling regime, we performed simulations of ideal lossless cavities ($\gamma_{\text{cav}} = 0$ ps⁻¹) containing between 32 and 512 Rhodamines, distributed evenly along the z axis (Fig. 1). In all simulations, the UP was excited initially at a fixed value of the wave vector (incidence angle), as indicated by the yellow circles in Fig. 3. Although in experiment, the ultra-short pump pulse required for such instantaneous excitation would have sufficient energy bandwidth to excite multiple states simultaneously, we here assume that the pulse is infinitely narrow in both energy and time (i.e., a δ -pulse), which significantly facilitates the interpretation of the trajectories.

In the first column of Fig. 3, we show the photo-absorption intensity as a function of both energy and wave vector for an optical cavity with 32, 64, and 512 molecules and a vacuum field strength of 0.0002 a.u. The Rabi splitting, defined as the energy gap between the two bright absorption branches at the wave vector where the cavity dispersion intersects the dispersionless absorption maximum of the Rhodamine molecules [white dashed lines, see also Fig. 2(b)], increases with the square root of the number of molecules, N , inside the mode volume ($\Omega_{\text{Rabi}} \propto \sqrt{N/V_{\text{cav}}}$, Table I).

Because the Rabi splitting of 919 meV for the ensemble with 512 molecules exceeds 20% of molecular excitation energy, this cavity system is no longer in the strong coupling (SC) regime but in the ultra-strong coupling (USC) regime.⁷¹ Although for such coupling strengths, the RWA may no longer be valid,^{72,73} the Tavis-Cummings model can still provide a qualitative description of the polariton dynamics.⁶⁸ For the purposes of this work, we include this cavity system to illustrate what happens if the UP is energetically well separated from the dark state manifold but refrain from interpreting the dynamics observed in this system further.

To keep the 512 molecule cavity within the SC regime, where the TC model is valid, without changing the total number of polaritonic (bright plus dark) states, we repeated the simulation with a vacuum field strength of 0.00007 a.u. (0.3 MV cm⁻¹). For comparison, we also performed a simulation of 256 Rhodamine molecules in this cavity. In the first column of Fig. 4, we show the photo-absorption spectra of these two systems. As for the cavities with the smaller mode volumes and hence stronger vacuum fields (Fig. 3), the Rabi splitting scales with the square root of the molecular concentration (Table I).

1. Population dynamics

As in previous simulation studies,^{37,38} we observe rapid population transfer from the bright UP into dark states, defined here as polaritonic states, ψ^m , for which the total contribution of the photonic cavity modes [Eq. (12)] is below a threshold, i.e., $\sum_{n=0}^{n_{\text{max}}} |\alpha_n^m|^2 < 0.05$. In the central panels of Fig. 3, the LP (pink), the UP (cyan), and the dark state (black) populations are plotted for ensembles of 32, 64, and 512 molecules inside an optical cavity with 16 modes and a vacuum field strength of 0.0002 a.u. (1 MV cm⁻¹). The central panels of Fig. 4 show this information for a cavity with a field strength of 0.00007 a.u. (0.3 MV cm⁻¹). The rapid decay from the UP into the dark state manifold is in line with the predictions by Agranovich and co-workers,²³ who estimated a timescale of ~ 50 fs for this process. The rather inefficient and slow population buildup of the LP, in particular, for larger N , has also been suggested in previous theoretical work.²⁸ Here, the 32 molecule cavity forms an exception due to the small N/n_{max} ratio, as will be discussed below.

For cavity systems with fewer molecules than modes (i.e., $N < n_{\text{max}}$), all states contain a significant photonic contribution ($\sum_{n=0}^{n_{\text{max}}} \alpha_n$), and thus, these systems lack a clear dark state manifold. In reality, the molecular density inside a micro-cavity exceeds the density of cavity modes by orders of magnitude³⁴ and the dark state manifold is very dense. We therefore only compare trends in the population dynamics of the dark and bright states for simulations in which $N > n_{\text{max}}$. For completeness, the results for cavities containing fewer molecules than modes are shown in the [supplementary material](#). As shown in the central columns of Figs. 3 and 4, the dark state population reaches a maximum shortly after the Rhodamine cavity is photo-excited into a point on the UP branch.

Because in the lossless cavities ($\gamma_{\text{cav}} = 0$) the bright states do not decay, the populations approach a dynamic equilibrium between the dark states, upper and lower polaritons. The relative occupancy of these states critically depends on the number of available dark states and thus on the N/n_{max} ratio. Indeed, for the smallest ensembles with 32 molecules or 64 molecules, the dark state population converges

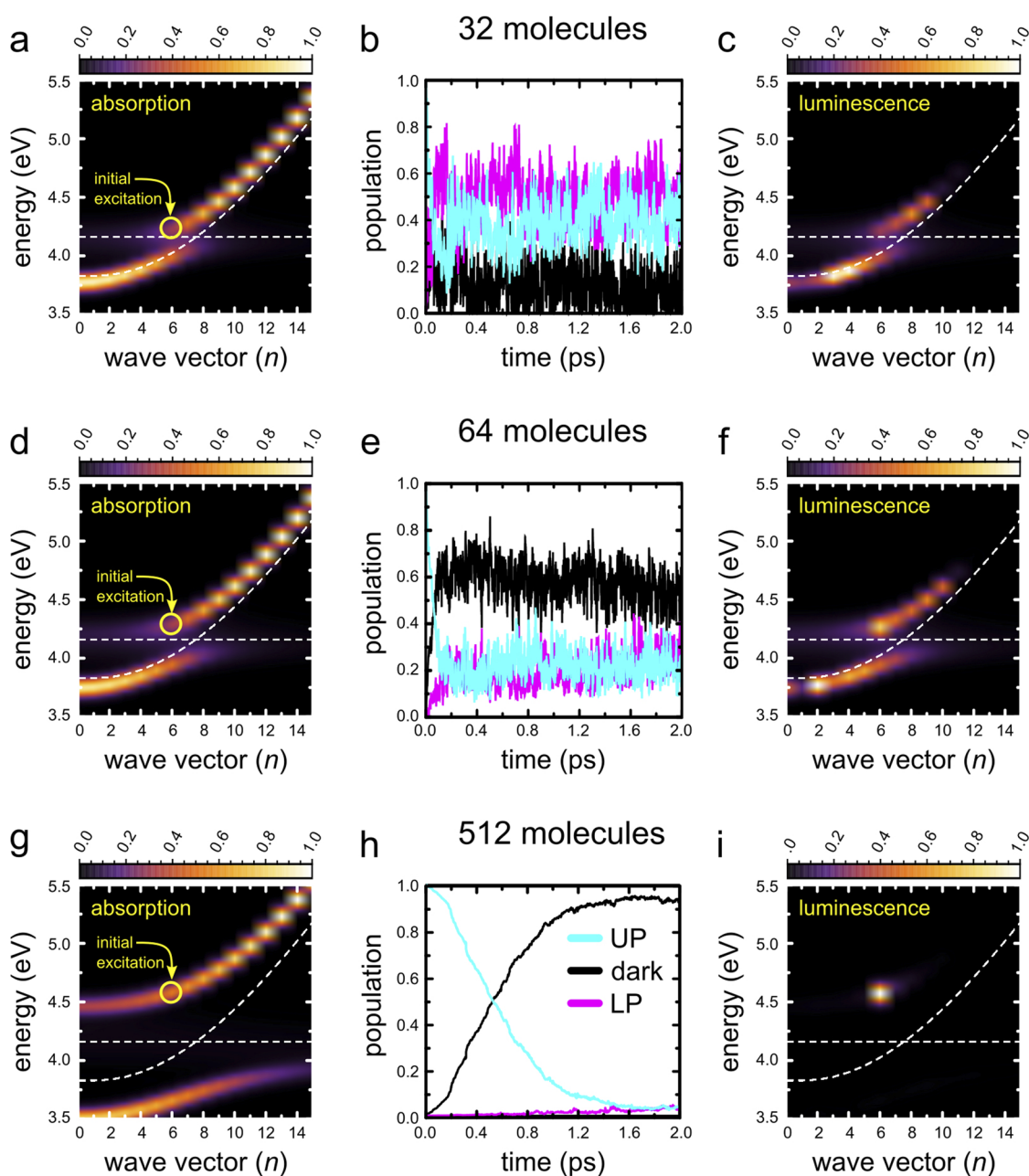


FIG. 3. Wave-vector (angle) resolved absorption spectra [(a), (d), and (g)], time-resolved populations of the upper polariton (UP), lower polariton (LP), and dark states [(b), (e), and (h)], and wave-vector resolved photo-luminescence spectra [(c), (f), and (i)] of Rhodamine-cavity systems with 32 [(a)–(c)], 64 [(d)–(f)], and 512 molecules [(g)–(i)]. The cavity has a vacuum field strength of 0.0002 a.u. (1 MV cm^{-1}) and an infinite Q-factor (i.e., $\gamma_{\text{cav}} = 0$). The cavity dispersion and molecular absorption maximum [Fig. 2(b)] are shown as white dashed lines. The points on the UP branch to which the systems were initially excited are indicated by yellow circles. The photo-luminescence spectra were obtained by accumulating the signal over the entire trajectories (2 ps).

to a value well below one, while both UP and LP remain significantly populated throughout the simulation [Figs. 3(b) and 3(e)]. In contrast, the dark state occupancy in the cavities with 256 and 512 molecules converges to near unity irrespective of the vacuum

field strength [Figs. 3(h) and 4(e)] or the number of molecules [Figs. 4(b) and 4(e)]. However, the rate at which equilibrium is reached in the larger cavity systems depends on the Rabi splitting and is lowest for the largest Rabi splitting of 919 meV [Fig. 3(h)]. The

TABLE I. Molecular ensembles strongly coupled to a cavity supporting 16 modes.

N	8	16	32	64	64 ^a	512	256	512
E (a.u.)	0.000 2	0.000 2	0.000 2	0.000 2	0.000 2	0.000 2	0.000 07	0.000 07
Ω_{Rabi} (meV)	115	163	230	325	325	919	228	322

^aRandomly distributed along the z axis.

rationale for this trend is that the strength of the non-adiabatic coupling between the UP and the dark states is inversely proportional to the energy gap [Eq. (13)], which increases with the Rabi splitting.

The same rationale holds for the subsequent relaxation from the dark state manifold into the LP, which is most efficient when the gap is small, as in the cavities filled with 32 or 64 molecules. In addition, the decay rate depends on the number of dark states. With many dark states available, as in the cavities containing 256 and 512 molecules, transitions into the LP compete with transitions among dark states. This effect is demonstrated by comparing

cavities with similar Rabi splitting but different numbers of molecules. In cavities with a vacuum field strength of 0.0002 a.u. and 32 or 64 molecules, the buildup of the LP populations is faster than in cavities with a vacuum field strength of 0.0007 a.u. and 256 or 512 molecules, despite comparable Rabi splittings.

2. Photo-luminescence

Although the wave vectors (k_z) of the dark states are not well defined, non-adiabatic coupling to bright polaritonic states with

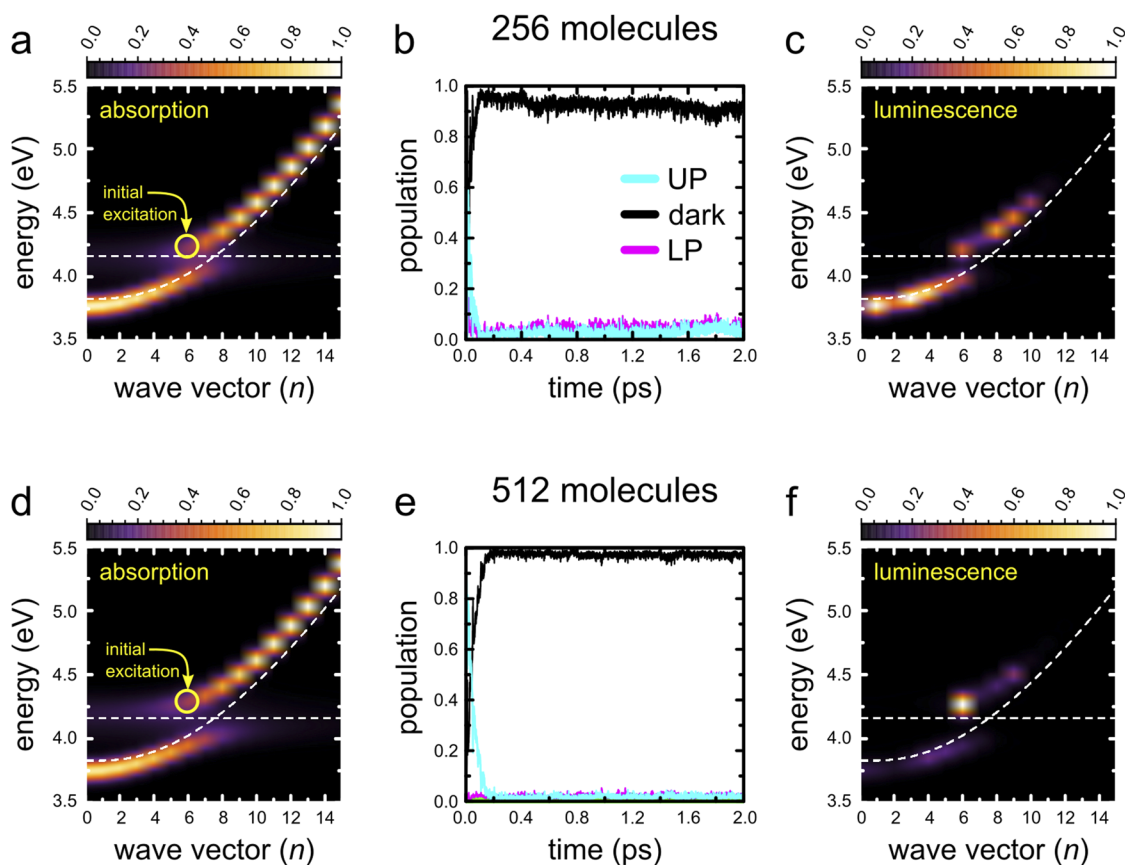


FIG. 4. Wave-vector (angle) resolved absorption spectra [(a) and (d)], time-resolved populations of the upper polariton (UP), lower polariton (LP), and dark states [(b) and (e)], and wave-vector resolved photo-luminescence spectra [(c) and (f)] of Rhodamine-cavity systems with 256 [(a)–(c)] and 512 molecules [(d)–(f)]. The cavity has a vacuum field strength of 0.000 07 a.u. (0.3 MV cm^{−1}) and an infinite Q-factor (i.e., $\gamma_{\text{cav}} = 0$). The cavity dispersion and molecular absorption maximum (see Fig. 2) are shown as white dashed lines. The points on the UP branch to which the systems were initially excited are indicated by yellow circles. The photo-luminescence spectra were obtained by accumulating the signal over the entire trajectories (2 ps).

well-defined wave vectors [i.e., the third and fourth terms on the RHS in Eq. (15) couple states *with* and *without* cavity mode excitation] can induce population transfer from the dispersionless dark states into bright states with a different k_z and energy compared to the point on the UP dispersion branch into which the system was initially excited. Experimentally, this relaxation process can be probed by recording angle-dependent photo-luminescence spectra.^{17,19–21,27} However, whereas in realistic cavities (discussed below), the bright polaritonic states emit their photon and only the dark states can have a long lifetime, in the ideal cavities considered here, both bright and dark states have infinite lifetimes, implying that photo-luminescence is not observable. To overcome this limitation of the lossless cavities in our simulations, we computed *hypothetical* photo-luminescence spectra instead by accumulating the “visibility,”¹⁸ defined as the weighted contribution of the cavity modes to the polaritonic states [i.e., $|c_m|^2 |\alpha_b^m|^2$, Eq. (24), with $m \in [1, N + n_{\text{max}} + 1]$] and normalizing the accumulated signal over the trajectories.

In the right panels of Figs. 3 and 4, we show the hypothetical angle-resolved photo-luminescence spectra accumulated during the 2 ps Ehrenfest trajectories of perfect cavities with various numbers of Rhodamine molecules. While 2 ps is many orders of magnitude shorter than the typical signal accumulation time in stationary photo-luminescence measurements, the observed trends are in qualitative agreement with such experiments. As in experiment, cavity photo-luminescence is observed from a wide range of angles all along the bright polaritonic branches, with significant emission from the LP at the smaller k_z -vectors for the smallest ensembles. Due to the much higher density of dark states in cavities with larger ensembles ($N \geq 256$), the transient population of the LP branch remains small. Therefore, only a very weak emission is observed from the LP branch in the larger ensembles. This observation is in line with a relaxation bottleneck for reaching the minimum on the LP branch, as observed in experiments.⁷⁴

Emission is not only observed at energies and wave vectors below the initial excitation but also at energies and wave vectors above the initial excitation. We speculate that this anti-Stokes

emission is predominantly caused by the relatively large energy fluctuations when small systems, like ours, are simulated at constant temperature. Therefore, even if anti-Stokes emission has been observed experimentally at the minimum of the lower polaritonic energy branch^{75,76} as well as emission from the UP at elevated temperatures,²⁷ we consider the photo-luminescence at the higher energies and k_z -vectors observed here, a finite size effect due to relatively large energy fluctuations in the small simulation systems, and hence do not consider this further.

Ignoring the visibility of the UP branch due to re-population from the dark states on the one hand and due to the short timescale of the simulation on the other hand, the spectra in combination with the evolution of the populations (central panels in Figs. 3 and 4) suggest ultra-fast relaxation from the UP into the dark state manifold followed by slower transitions from the dark states into the LP branch. While dark states do not have well-defined wave vectors, their non-adiabatic coupling to bright states with well-defined wave vectors depends mostly on the energy gap. Therefore, these couplings connect the dispersion-less dark state manifold to the LP branch over the complete range of wave vectors. As the LP energy is bound by the minimum of the cavity dispersion at $k_z = 0$, the population eventually ends up there. Because the size of the dark state manifold is determined by the number of Rhodamine molecules, we only observe relaxation into that minimum within the 2 ps simulation time for the smaller systems (i.e., $N \leq 256$).

3. Positional disorder

While varying the initial atomic velocities at the start of the simulations rapidly introduced disorder among the molecular excitation energies, the molecules were located at equally spaced distances along the z axis, introducing a periodic ordering that would be difficult to achieve experimentally in polymer-based micro-cavities. Inside such media, the molecules are randomly distributed instead. To also mimic the latter situation in our simulations, we distributed 64 Rhodamine molecules by adding random displacements to the

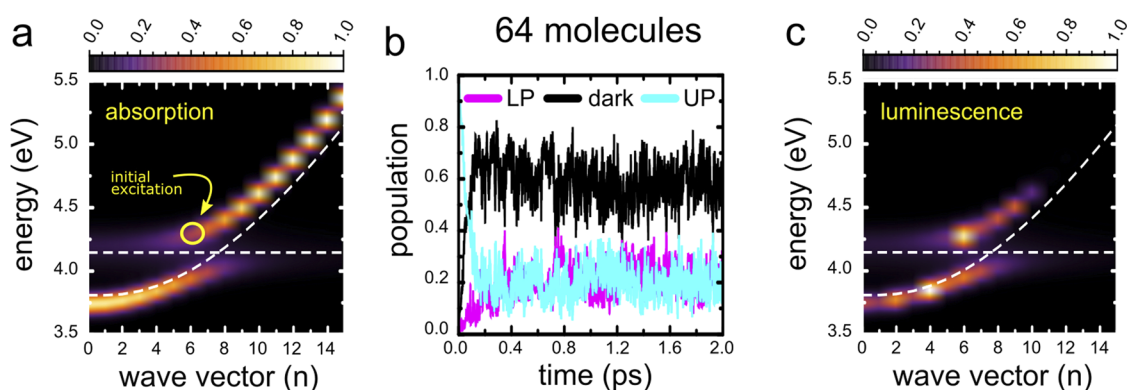


FIG. 5. Wave-vector (angle) resolved absorption spectra (a), time-resolved populations of upper polariton (UP), lower polariton (LP), and dark states (b), and wave-vector resolved photo-luminescence spectra (c) of a Rhodamine-cavity system with 64 molecules, positioned randomly along the z axis of the cavity. The cavity has a vacuum field strength of 0.0002 a.u. (1 MV cm⁻¹) and an infinite Q-factor (i.e., $\gamma_{\text{cav}} = 0$). The cavity dispersion and molecular absorption maximum (see Fig. 2) are shown as white dashed lines. The point on the UP branch to which the system was initially excited is indicated by a yellow circle. The photo-luminescence spectra were obtained by accumulating the signal over the entire, 2 ps, trajectory.

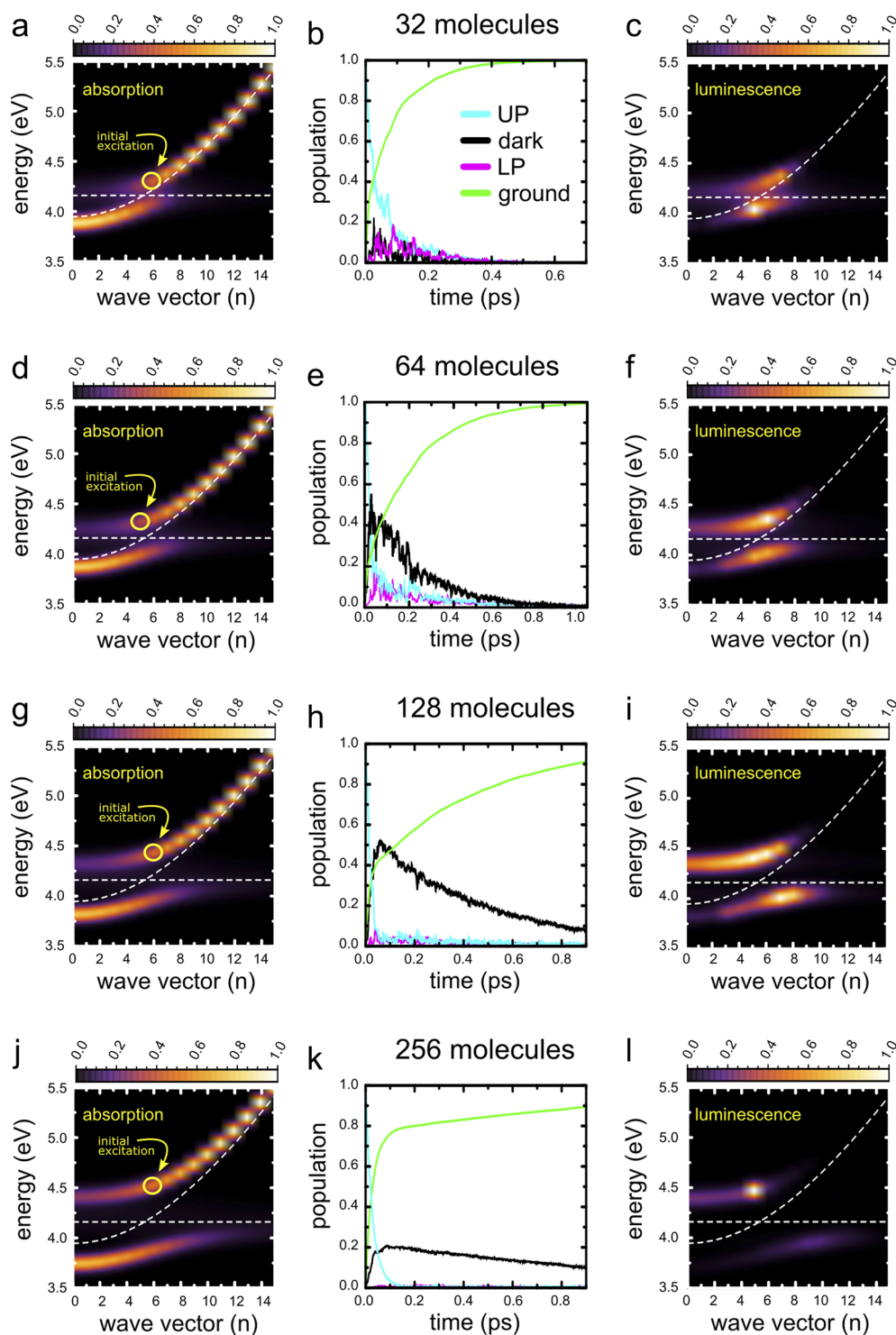


FIG. 6. Wave-vector (angle) resolved absorption spectra [(a), (d), (g), and (j)], time-resolved populations of upper polariton (UP), lower polariton (LP), and dark states [(b), (e), (h), and (k)], and wave-vector resolved photo-luminescence spectra [(c), (f), (i), and (l)] of Rhodamine-cavity systems with 32 [(a)–(c)], 64 [(d)–(f)], 128 [(g)–(i)], and 256 molecules [(j)–(l)]. The cavity has a vacuum field strength of 0.0002 a.u. (1 MV cm^{-1}) and a Q-factor of $\gamma_{\text{cav}} = 66.7 \text{ ps}^{-1}$. The cavity dispersion and molecular absorption maximum (see Fig. 2) are shown as white dashed lines. The points on the UP branch to which the systems were initially excited are indicated by a yellow circle. The photo-luminescence spectra were obtained by accumulating the signal over the final 0.9 ps of the trajectories.

z -coordinates of their geometrical centers while keeping the molecules aligned between the mirrors of the cavity (i.e., $x_j = y_j = 0$), where the vacuum field has the highest strength (Fig. 1). As before, 16 modes were included, and the vacuum field strength was set to 0.0002 a.u. (1 MV cm^{-1}).

The angle-resolved absorption and luminescence (“visibility”) spectra of these cavities, shown in Fig. 5, are very similar to the spectra obtained for the cavity system with 64 evenly distributed molecules (middle row in Fig. 3). In addition, the evolution of the populations in the bright and dark states closely resembles that of the cavity with regularly spaced molecules [Fig. 3(f)]. Based on these similarities, we conclude that the relaxation process is not significantly influenced by positional disorder of molecules. As before, rapid decay of the excitation from a point on the bright UP branch into the dispersion-less dark state manifold is followed by much slower decay into the bright LP branch, where it eventually accumulates near the minimum of the branch at $k_z = 0$.

B. Molecules in lossy cavities

While we so far considered ideal *lossless* cavities, without photonic decay, and thus an infinitely high Q-factor, experiments are normally done in low-Q cavities with photonic lifetimes on the order of tens of femtoseconds. To investigate the effect of cavity photon loss on the relaxation dynamics, we repeated the simulations of 32, 64, 128, and 256 Rhodamine molecules in a Fabry–Pérot cavity with a decay rate of $\gamma_{\text{cav}} = 66.7 \text{ ps}^{-1}$ or $\tau_{\text{cav}} = 15 \text{ fs}$ [Eq. (20)], a value in line with previous experiments.^{52,53}

Including cavity dissipation adds a direct relaxation channel into the ground state ($|S_0^0 S_0^2 \dots S_0^N\rangle|0\rangle$). As demonstrated by the rapid buildup of ground state populations in the central column of Fig. 6, direct photo-emission from the UP competes with non-adiabatic relaxation into the dark state manifold, leading to a much smaller total population of the latter. In addition, and in contrast to the ideal lossless cavities, where the transitions between the dark and bright states were reversible, direct photo-emission from the LP branch gradually depletes the dark state manifold. Therefore, the total population of the dark states not only reaches a much lower value in the lossy cavities but also decays with time.

The ultra-fast rise of the ground-state at the expense of the UP state suggests that emission is predominately observed from where the initial excitation took place. Experimentally, however, such emission would be very difficult to measure due to the overlap between the excitation and detection wavelengths, in both stationary and transient spectroscopy setups. With typical instrument response functions (IRF) on the order of tens of femtoseconds, time-resolved spectroscopy techniques furthermore lack the time resolution required to observe the ultra-fast transient initial emission from the UP. To approximately account for these effects, we omitted the first 100 fs in the photo-luminescence spectra in the right side column of Fig. 6.

As in the lossless cavities, the dark states lack a well-defined wave vector, and therefore, transitions from these dark states into the bright polaritonic states can occur over the full wave-vector range. However, in contrast to the lossless cavities, where emission was predominantly observed near the minimum of the LP branch at $k_z = 0$, we observe that emission from the bright polaritons in the lossy cavities mostly occurs at energy levels near the dark state

manifold. We speculate that the enhanced photo-luminescence intensity at higher energies in the cavities with finite photon lifetimes as compared to the ideal cavities with an infinite lifetime is due to ultra-fast photon emission from the bright polaritonic states, which competes with the much slower non-adiabatic relaxation through the dark state manifold into the LP branch at lower energies and wave vectors. Rather than returning into the dark state manifold, population entering or re-entering the bright polaritonic states quickly decays instead through photon emission. Because the non-adiabatic coupling is highest for bright states near the maximum of the dark state distribution, the emission dominates from those states.

Previously, enhanced decay into the LP was observed at k -vectors where the energy gap between the molecular absorption maximum and the LP matches specific Raman-active vibrational modes.^{15,23,77} While our model includes the non-adiabatic coupling connecting those vibrational modes to the polaritonic transitions [Eq. (13)], the classical treatment of the vibrational dynamics in combination with the Ehrenfest formalism causes continuous energy exchange rather than discrete on-resonance quantum jumps. We therefore do not observe such enhancements in our simulations.

V. CONCLUSION AND OUTLOOK

Before strong light–matter coupling between confined light modes and molecules can be exploited for chemistry or other applications, a full understanding of the effects of polariton formation on the underlying molecular dynamics of the strongly coupled molecules is needed. To provide the required atomistic insights, we developed a multi-scale molecular dynamics method for simulating molecules in optical cavities with chemical accuracy.³⁶ While we could couple an arbitrary number of molecules to a *single* cavity mode in the initial implementation, we have now extended our model to an arbitrary number of modes, which improves the description of the micro-cavity in our simulations. With this extension, our model can better capture experiments performed on large numbers of molecules in low-finesse cavity systems with multiple modes, as compared to previous models of strong light–matter coupling, which either omit important chemical details, focus on a single molecule, or include only one confined light mode, often with an infinite lifetime.

To demonstrate this new functionality, we have simulated the relaxation dynamics of large ensembles of realistic molecules strongly coupled to a red-detuned optical micro-cavity with a realistic mode structure that captures the cavity dispersion. The results of these simulations suggest that resonant excitation of the molecule–cavity system into the UP at a fixed incidence angle is immediately followed by ultra-fast relaxation into the dark state manifold.²³ Despite the lack of a clear wave-vector dependence, the dark states can subsequently decay into the optically bright polaritonic states with wave-vector dependence. Therefore, photo-luminescence is observed from the LP branch, accumulating at small wave vectors, where the energy is lowest.

Our computational results thus confirm theoretical predictions that relaxation within the dark state manifold, also called the exciton reservoir, is essential to reach the bottom of the LP branch in

optically excited molecule–cavity systems.^{23,28,33} Without group velocity, and because of the quasi-bosonic nature of polaritons, condensation at this minimum can occur, which is essential for polaritonic lasing with organic molecules.^{78–80} Although the restriction to the single excitation subspace precludes the modeling of the actual condensation, we can track the relaxation process at the atomistic level. Therefore, our work could pave the way to systematically investigate the effects of molecular structure and environment on the efficiency of polariton condensation and hence contribute to a rational optimization of cavity parameters for polaritonic lasing with organic molecules.

SUPPLEMENTARY MATERIAL

See the [supplementary material](#) for simulation workflow; wave vector (angle) resolved absorption spectra, time-resolved populations of upper polariton (UP), lower polariton (LP), and dark states, and wave vector resolved photo-luminescence spectra of ideal lossless cavities containing 8 and 16 Rhodamines; and quicktime animation of time-resolved photo-luminescence from a lossless cavity containing 32 Rhodamines.

ACKNOWLEDGMENTS

The authors thank D. Morozov and J. J. Toppari for commenting on this manuscript and many fruitful discussions. This work was supported by the Academy of Finland (Grant No. 323996 to G.G.) as well as the European Research Council (Grant No. ERC-2016-StG-714870 to J.F.) and the Spanish Ministry for Science, Innovation, and Universities—AEI (Grant No. RTI2018-099737-B-I00 to J.F.). We thank the Center for Scientific Computing (CSC-IT Center for Science) for generous computational resources.

DATA AVAILABILITY

The data that support the findings of this study are available from the corresponding author upon reasonable request.

REFERENCES

- J. A. Hutchison, T. Schwartz, C. Genet, E. Devaux, and T. W. Ebbesen, “Modifying chemical landscapes by coupling to vacuum fields,” *Angew. Chem., Int. Ed.* **51**, 1592–1596 (2012).
- A. Thomas, J. George, A. Shalabney, M. Dryzhakov, S. J. Varma, J. Moran, T. Chervy, X. Zhong, E. Devaux, C. Genet, J. A. Hutchison, and T. W. Ebbesen, “Ground-state chemical reactivity under vibrational coupling to the vacuum electromagnetic field,” *Angew. Chem., Int. Ed.* **55**, 11462–11466 (2016).
- K. Stranius, M. Herzog, and K. Börjesson, “Selective manipulation of electronically excited states through strong light-matter interactions,” *Nat. Commun.* **9**, 2273 (2018).
- B. Munkhbat, M. Wersäll, D. G. Baranov, T. J. Antosiewicz, and T. Shegai, “Suppression of photo-oxidation of organic chromophores by strong coupling to plasmonic nanoantennas,” *Sci. Adv.* **4**, eaas9552 (2018).
- A. Thomas, L. Lethuillier-Karl, K. Nagarajan, R. M. A. Vergauwe, J. George, T. Chervy, A. Shalabney, E. Devaux, J. Moran, and T. W. Ebbesen, “Tilting a ground-state reactivity landscape by vibrational strong coupling,” *Science* **363**, 615–619 (2019).
- J. Lather, P. Bhatt, A. Thomas, T. W. Ebbesen, and J. George, “Cavity catalysis by cooperative vibrational strong coupling of reactant and solvent molecules,” *Angew. Chem., Int. Ed.* **58**, 10635–10638 (2019).
- R. M. A. Vergauwe, A. Thomas, K. Nagarajan, A. Shalabney, J. George, T. Chervy, M. Seidel, E. Devaux, V. Torbeev, and T. W. Ebbesen, “Cavity catalysis by cooperative vibrational strong coupling of reactant and solvent molecules,” *Angew. Chem., Int. Ed.* **58**, 15324–15328 (2019).
- H. Mabuchi and A. C. Doherty, “Cavity quantum electrodynamics: Coherence in context,” *Science* **298**, 1372–1377 (2002).
- P. Törmä and W. L. Barnes, “Strong coupling between surface plasmon polaritons and emitters: A review,” *Rep. Prog. Phys.* **78**, 013901 (2015).
- T. W. Ebbesen, “Hybrid light-matter states in a molecular and material science perspective,” *Acc. Chem. Res.* **49**, 2403–2412 (2016).
- J. Feist, J. Galego, and F. J. Garcia-Vidal, “Polaritonic chemistry with organic molecules,” *ACS Photonics* **5**, 205–216 (2018).
- A. Armitage, M. S. Skolnick, V. N. Astratov, D. M. Whittaker, G. Panzarini, L. C. Andreani, T. A. Fisher, J. S. Roberts, A. V. Kavokin, M. A. Kaliteevski, and M. R. Vladimirova, “Optically induced splitting of bright excitonic states in coupled quantum microcavities,” *Phys. Rev. B* **57**, 14877–14881 (1998).
- J. H. Burroughes, D. D. C. Bradley, A. R. Brown, R. N. Marks, K. Mackay, R. H. Friend, P. L. Burns, and A. B. Holmes, “Light-emitting diodes based on conjugated polymers,” *Nature* **347**, 539–541 (1990).
- D. G. Lidzey, D. D. C. Bradley, S. J. Martin, and M. A. Pate, “Pixelated multicolor microcavity displays,” *IEEE J. Sel. Top. Quantum Electron.* **4**, 113–118 (1998).
- D. G. Lidzey, D. D. C. Bradley, M. S. Skolnick, T. Virgili, S. Walker, and D. M. Whittaker, “Strong exciton-photon coupling in an organic semiconductor microcavity,” *Nature* **395**, 53–55 (1998).
- D. G. Lidzey, T. Virgili, D. D. C. Bradley, M. S. Skolnick, S. Walker, and D. M. Whittaker, “Observation of strong exciton-photon coupling in semiconductor microcavities containing organic dyes and J-aggregates,” *Opt. Mater.* **12**, 243–247 (1999).
- D. G. Lidzey, D. D. C. Bradley, T. Virgili, A. Armitage, M. S. Skolnick, and S. Walker, “Room temperature polariton emission from strongly coupled organic semiconductor microcavities,” *Phys. Rev. Lett.* **82**, 3316–3319 (1999).
- D. G. Lidzey, D. Bradley, A. Armitage, S. Walker, and M. Skolnick, “Photon-mediated hybridization of Frenkel excitons in organic semiconductor microcavities,” *Science* **288**, 1620–1623 (2000).
- D. Lidzey, A. Fox, M. Rahn, M. Skolnick, V. Agranovich, and S. Walker, “Experimental study of light emission from strongly coupled organic semiconductor microcavities following nonresonant laser excitation,” *Phys. Rev. B* **65**, 195312-1–195312-10 (2002).
- J.-H. Song, Y. He, A. Nurmikko, J. Tischler, and V. Bulovic, “Exciton-polariton dynamics in a transparent organic semiconductor microcavity,” *Phys. Rev. B* **69**, 235330 (2004).
- G. Lodden and R. Holmes, “Electrical excitation of microcavity polaritons by radiative pumping from a weakly coupled organic semiconductor,” *Phys. Rev. B* **82**, 125317 (2010).
- D. M. Coles, P. Michetti, C. Clark, W. C. Tsoi, A. M. Adawi, J.-S. Kim, and D. G. Lidzey, “Vibrationally assisted polariton-relaxation processes in strongly coupled organic-semiconductor microcavities,” *Adv. Funct. Mater.* **21**, 3691–3696 (2011).
- V. M. Agranovich, M. Litinskaia, and D. G. Lidzey, “Cavity polaritons in microcavities containing disordered organic semiconductors,” *Phys. Rev. B* **67**, 085311 (2003).
- V. M. Agranovich and G. C. La Rocca, “Electronic excitations in organic microcavities with strong light-matter coupling,” *Solid State Commun.* **135**, 544–553 (2005).
- V. Agranovich and Y. Gartstein, “Nature and dynamics of low-energy exciton polaritons in semiconductor microcavities,” *Phys. Rev. B* **75**, 075302 (2007).
- M. Litinskaya, “Propagation and localization of polaritons in disordered organic microcavities,” *Phys. Lett. A* **372**, 3898–3903 (2008).
- D. M. Coles, P. Michetti, C. Clark, A. M. Adawi, and D. G. Lidzey, “Temperature dependence of the upper-branch polariton population in an organic semiconductor microcavity,” *Phys. Rev. B* **84**, 205214 (2011).

- ²⁸M. Litinskaya, P. Reineker, and V. M. Agranovich, "Fast polariton relaxation in strongly coupled organic microcavities," *J. Lumin.* **110**, 364–372 (2004).
- ²⁹P. Michetti and G. C. La Rocca, "Polariton states in disordered organic microcavities," *Phys. Rev. B* **71**, 115320 (2005).
- ³⁰P. Michetti and G. C. La Rocca, "Simulation of J-aggregate microcavity photoluminescence," *Phys. Rev. B* **77**, 195301 (2008).
- ³¹P. Michetti and G. C. La Rocca, "Exciton-phonon scattering and photoexcitation dynamics in J-aggregate microcavities," *Phys. Rev. B* **79**, 35325 (2009).
- ³²P. Michetti and G. C. La Rocca, "Polariton-polariton scattering in organic microcavities at high excitation densities," *Phys. Rev. B* **82**, 115327 (2010).
- ³³M. Litinskaya and P. Reineker, "Balance between incoming and outgoing cavity polaritons in a disordered organic microcavity," *J. Lumin.* **122–123**, 418–420 (2007).
- ³⁴J. d. Pino, J. Feist, and F. J. Garcia-Vidal, "Quantum theory of collective strong coupling of molecular vibrations with a microcavity mode," *New J. Phys.* **17**, 053040 (2015).
- ³⁵K. B. Arnardottir, A. J. Moilanen, A. Strashko, P. Törmä, and J. Keeling, "Multimode organic polariton lasing," *Phys. Rev. Lett.* **125**, 233603 (2020).
- ³⁶H. L. Luk, J. Feist, J. J. Toppari, and G. Groenhof, "Multiscale molecular dynamics simulations of polaritonic chemistry," *J. Chem. Theory Comput.* **13**, 4324–4335 (2017).
- ³⁷J. del Pino, F. A. Y. N. Schröder, A. W. Chin, J. Feist, and F. J. Garcia-Vidal, "Tensor network simulation of non-Markovian dynamics in organic polaritons," *Phys. Rev. Lett.* **121**, 227401 (2018).
- ³⁸G. Groenhof, C. Climent, J. Feist, D. Morozov, and J. J. Toppari, "Tracking polariton relaxation with multiscale molecular dynamics simulations," *J. Chem. Phys. Lett.* **10**, 5476–5483 (2019).
- ³⁹O. Vendrell, "Collective Jahn-Teller interactions through light-matter coupling in a cavity," *Phys. Rev. Lett.* **121**, 253001 (2018).
- ⁴⁰F. Herrera and F. C. Spano, "Dark vibronic polaritons and the spectroscopy of organic microcavities," *Phys. Rev. Lett.* **118**, 223601 (2017).
- ⁴¹F. Herrera and F. C. Spano, "Absorption and photoluminescence in organic cavity QED," *Phys. Rev. A* **95**, 053867 (2017).
- ⁴²A. Warshel and M. Levitt, "Theoretical studies of enzymatic reactions: Dielectric, electrostatic and steric stabilization of carbonium ion in the reaction of lysozyme," *J. Mol. Biol.* **103**, 227–249 (1976).
- ⁴³E. T. Jaynes and F. W. Cummings, "Comparison of quantum and semiclassical radiation theories with to the beam maser," *Proc. IEEE* **51**, 89–109 (1963).
- ⁴⁴M. Tavis and F. W. Cummings, "Approximate solutions for an N-molecule radiation-field Hamiltonian," *Phys. Rev.* **188**, 692–695 (1969).
- ⁴⁵A. Sisto, D. R. Glowacki, and T. J. Martínez, "Ab initio nonadiabatic dynamics of multichromophore complexes: A scalable graphical-processing-unit-accelerated exciton framework," *Acc. Chem. Res.* **47**, 2857–2866 (2014).
- ⁴⁶J. C. Tully, "Molecular dynamics with electronic transitions," *J. Chem. Phys.* **93**, 1061–1071 (1990).
- ⁴⁷R. Crespo-Otero and M. Barbatti, "Recent advances and perspectives on nonadiabatic mixed quantum-classical dynamics," *Chem. Rev.* **118**, 7026–7068 (2018).
- ⁴⁸G. Groenhof and J. J. Toppari, "Coherent light harvesting through strong coupling to confined light," *J. Phys. Chem. Lett.* **9**, 4848–4851 (2018).
- ⁴⁹P. Ehrenfest, "Bemerkung über die angenäherte gültigkeit der klassischen mechanik innerhalb der quantenmechanik," *Z. Phys.* **45**, 445–457 (1927).
- ⁵⁰G. Granucci, M. Persico, and A. Toniolo, "Direct semiclassical simulation of photochemical processes with semiempirical wave functions," *J. Chem. Phys.* **114**, 10608–10615 (2001).
- ⁵¹K. J. Vahala, "Optical microcavities," *Nature* **424**, 839–846 (2003).
- ⁵²T. Schwartz, J. A. Hutchison, J. Léonard, C. Genet, S. Haacke, and T. W. Ebbesen, "Polariton dynamics under strong light-molecule coupling," *ChemPhysChem* **14**, 125–131 (2013).
- ⁵³J. George, S. Wang, T. Chervy, A. Canaguier-Durand, G. Schaeffer, J.-M. Lehn, J. A. Hutchison, C. Genet, and T. W. Ebbesen, "Ultra-strong coupling of molecular materials: Spectroscopy and dynamics," *Faraday Discuss.* **178**, 281–294 (2015).
- ⁵⁴Y. Duan, C. Wu, S. Chowdhury, M. C. Lee, G. Xiong, W. Zhang, R. Yang, P. Cieplak, R. Luo, T. Lee, J. Caldwell, J. Wang, and P. Kollman, "A point-charge force field for molecular mechanics simulations of proteins based on condensed-phase quantum mechanical calculations," *J. Comput. Chem.* **24**, 1999–2012 (2003).
- ⁵⁵W. L. Jorgensen, J. Chandrasekhar, J. D. Madura, R. W. Impey, and M. L. Klein, "Comparison of simple potential functions for simulation liquid water," *J. Chem. Phys.* **79**, 926–935 (1983).
- ⁵⁶H. J. C. Berendsen, J. P. M. Postma, W. F. van Gunsteren, A. DiNola, and J. R. Haak, "Molecular dynamics with coupling to an external bath," *J. Chem. Phys.* **81**, 3684–3690 (1984).
- ⁵⁷B. Hess, H. Bekker, H. J. C. Berendsen, and J. G. E. M. Fraaije, "LINCS: A linear constraint solver for molecular simulations," *J. Comput. Chem.* **18**, 1463–1472 (1997).
- ⁵⁸S. Miyamoto and P. A. Kollman, "SETTLE: An analytical version of the SHAKE and RATTLE algorithms for rigid water molecules," *J. Comput. Chem.* **13**, 952–962 (1992).
- ⁵⁹U. Essmann, L. Perera, M. L. Berkowitz, T. Darden, H. Lee, and L. G. Pedersen, "A smooth particle mesh Ewald potential," *J. Chem. Phys.* **103**, 8577–8592 (1995).
- ⁶⁰E. Runge and E. K. U. Gross, "Density-functional theory for time-dependent systems," *Phys. Rev. Lett.* **52**, 997–1000 (1984).
- ⁶¹B. O. Roos, "Theoretical studies of electronically excited states of molecular systems using multiconfigurational perturbation theory," *Acc. Chem. Res.* **32**, 137–144 (1999).
- ⁶²A. A. Granovsky, "Extended multi-configuration quasi-degenerate perturbation theory: The new approach to multi-state multi-reference perturbation theory," *J. Chem. Phys.* **134**, 214113 (2011).
- ⁶³B. Hess, C. Kutzner, D. van der Spoel, and E. Lindahl, "GROMACS 4: Algorithms for highly efficient, load-balanced, and scalable molecular simulation," *J. Chem. Theory Comput.* **4**, 435–447 (2008).
- ⁶⁴I. S. Ufimtsev and T. J. Martínez, "Quantum chemistry on graphical processing units. 3. Analytical energy gradients and first principles molecular dynamics," *J. Chem. Theory Comput.* **5**, 2619–2628 (2009).
- ⁶⁵A. V. Titov, I. S. Ufimtsev, N. Luehr, and T. J. Martínez, "Generating efficient quantum chemistry codes for novel architectures," *J. Chem. Theory Comput.* **9**, 213–221 (2013).
- ⁶⁶G. Zengin, M. Wersäll, S. Nilsson, T. J. Antosiewicz, M. Käll, and T. Shegai, "Realizing strong light-matter interactions between single-nanoparticle plasmons and molecular excitons at ambient conditions," *Phys. Rev. Lett.* **114**, 157401 (2015).
- ⁶⁷D. Melnikau, R. Esteban, D. Savateeva, A. Sánchez-Iglesias, M. Grzelczak, M. K. Schmidt, L. M. Liz-Marzán, J. Aizpurua, and Y. P. Rakovich, "Rabi splitting in photoluminescence spectra of hybrid systems of gold nanorods and J-aggregates," *J. Phys. Chem. Lett.* **7**, 354–362 (2016).
- ⁶⁸C. A. Delpo, B. Kudisch, K. H. Park, S.-U.-Z. Khan, F. Fassio, D. Fausti, B. P. Rand, and G. D. Scholes, "Polariton transitions in femtosecond transient absorption studies of ultrastrong light-molecule coupling," *J. Phys. Chem. Lett.* **11**, 2667–2674 (2020).
- ⁶⁹M. J. Frisch, G. W. Trucks, H. B. Schlegel, G. E. Scuseria, M. A. Robb, J. R. Cheeseman, G. Scalmani, V. Barone, G. A. Petersson, H. Nakatsuji, K. Li, M. Caricato, A. V. Marenich, J. Bloino, B. G. Janesko, R. Gomperts, B. Mennucci, H. P. Hratchian, J. V. Ortiz, A. F. Izmaylov, J. L. Sonnenberg, D. Williams-Young, F. Ding, F. Lipparini, F. Egidi, J. Goings, B. Peng, A. Petrone, T. Henderson, D. Ranasinghe, V. G. Zakrzewski, J. Gao, N. Rega, G. Zheng, W. Liang, M. Hada, M. Ehara, K. Toyota, R. Fukuda, J. Hasegawa, M. Ishida, T. Nakajima, Y. Honda, O. Kitao, H. Nakai, T. Vreven, K. Throssell, J. A. Montgomery, Jr., J. E. Peralta, F. Ogliaro, M. J. Bearpark, J. J. Heyd, E. N. Brothers, K. N. Kudin, V. N. Staroverov, T. A. Keith, R. Kobayashi, J. Normand, K. Raghavachari, A. P. Rendell, J. C. Burant, S. S. Iyengar, J. Tomasi, M. Cossi, J. M. Millam, M. Klene, C. Adamo, R. Cammi, J. W. Ochterski, R. L. Martin, K. Morokuma, O. Farkas, J. B. Foresman, and D. J. Fox, Gaussian 16 Revision C.01, Gaussian, Inc., Wallingford, CT, 2016.
- ⁷⁰Mathematica, Version 11.3, Wolfram Research, Inc., Champaign, IL, 2018.
- ⁷¹P. Forn-Díaz, L. Lamata, E. Rico, J. Kono, and E. Solano, "Ultrastrong coupling regimes of light-matter interaction," *Rev. Mod. Phys.* **91**, 025005 (2019).

- ⁷²J. Flick, H. Appel, M. Ruggenthaler, and A. Rubio, "Cavity Born-Oppenheimer approximation for correlated electron-nuclear-photon systems," *J. Chem. Theory Comput.* **13**, 1616–1625 (2017).
- ⁷³J. Flick, M. Ruggenthaler, H. Appel, and A. Rubio, "Atoms and molecules in cavities: From weak to strong coupling in QED chemistry," *Proc. Natl. Acad. Sci. U. S. A.* **114**, 3026–3034 (2017).
- ⁷⁴D. M. Coles, R. Grant, D. G. Lidzey, C. Clark, and P. G. Lagoudakis, "Imaging the polariton relaxation bottleneck in strongly coupled organic semiconductor microcavities," *Phys. Rev. B* **88**, 121303 (2013).
- ⁷⁵K. Georgiou, R. Jayaprakash, A. Askitopoulos, D. M. Coles, P. G. Lagoudakis, and D. G. Lidzey, "Generation of anti-Stokes fluorescence in a strongly coupled organic semiconductor microcavity," *ACS Photonics* **5**, 4343–4351 (2018).
- ⁷⁶S. Takahashi and K. Watanabe, "Decoupling from a thermal bath via molecular polariton formation," *J. Phys. Chem. Lett.* **11**, 1349–1356 (2020).
- ⁷⁷V. Agranovich, H. Benisty, and C. Weisbuch, "Organic and inorganic quantum wells in a microcavity: Frenkel-Wannier-Mott excitons hybridization and energy transformation," *Solid State Commun.* **102**, 631–636 (1997).
- ⁷⁸S. Kéna-Cohen and S. R. Forrest, "Room-temperature polariton lasing in an organic single-crystal microcavity," *Nat. Photonics* **4**, 371–375 (2010).
- ⁷⁹K. S. Daskalakis, S. A. Maier, R. Murray, and S. Kéna-Cohen, "Nonlinear interactions in an organic polariton condensate," *Nat. Mater.* **13**, 271–275 (2014).
- ⁸⁰J. Keeling and S. Kéna-Cohen, "Bose-Einstein condensation of exciton-polaritons in organic microcavities," *Annu. Rev. Phys. Chem.* **71**, 435–459 (2020).